Published in final edited form as:
J Struct Biol. 2010 May ; 170(2): 406–412. doi:10.1016/j.jsb.2009.12.012.

Non-equilibrium Silk Fibroin Adhesives

Tuna Yucel[1], **Nikola Kojic**[1], **Gary G. Leisk**[2], **Tim J. Lo**[1], and **David L. Kaplan**[1]
[(1)]Department of Biomedical Engineering Tufts University, Medford, MA 02155 (U.S.A.)
[(2)]Department of Mechanical Engineering Tufts University, Medford, MA 02155 (U.S.A.)

Abstract

Regenerated silkworm silk solutions formed metastable, soft-solid-like materials (e-gels) under weak electric fields, displaying interesting mechanical characteristics such as dynamic adhesion and strain stiffening. Raman spectroscopy, in situ electric field dynamic oscillatory rheology and polarized optical microscopy indicated that silk fibroin electrogelation involved intermolecular self-assembly of silk molecules into amorphous, micron-scale, micellar structures and the formation of relatively long lifetime, intermicellar entanglement crosslinks. Overall, the electrogelation process did not require significant intramolecular β-strand or intermolecular β-sheet formation, unlike silk hydrogels. The kinetics of e-gel formation could be tuned by changing the field strength and assembly conditions, such as silk concentration and solution pH, while e-gel stiffness was partially reversible by removal of the applied field. Transient adhesion testing indicated that the adhesive characteristics of e-gels could at least partially be attributed to a local increase in proton concentration around the positive electrode due to the applied field and surface effects. A working model of electrogelation was described en route to understanding the origins of the adhesive characteristics.

Keywords

silkworm silk; electrogelation; rheology; adhesion; structure

1. Introduction

Recently, there has been increasing interest in utilizing the electric field responsive assembly of biopolymers for biomaterials applications [1–3]. However, most research efforts have concentrated on “apparent equilibrium” state properties/applications of these systems. For example, Akkus et al. applied weak DC fields to synthesize dense and oriented collagen constructs and studied the biophysical characteristics of these scaffolds for tissue/ligament repair [1]. Servoli and coworkers employed small amplitude AC fields to enforce orientation of silk fibroin molecules for anisotropic film processing to induce directional spreading of MRC5 fibroblasts [3]. We have recently discovered that the silk fibroin aqueous solutions transition into a “non-equilibrium”, soft-solid-like material (electrogel or e-gel) via application of DC electric fields on the order of a few tens of V/mm [2]. This system

Correspondence: David L. Kaplan Department of Biomedical Engineering Science and Technology Center 4 Colby Street, Medford, MA 02155 david.kaplan@tufts.edu Tel: 617-627-3251 Fax: 617-627-3231.

displays unique, viscoelastic and adhesive properties suggesting prospects for biomedical applications.

Silk fibroin, the structural, self-assembling protein of silkworm fibers is a high molecular weight block copolymer consisting of a heavy (≈ 370 kDa) and light (≈ 26 kDa) chain with varying amphiphilicity linked by a single disulfide bond [4]. The heavy chain consists of alternating arrays of 12 repetitive oligo-peptide domains that are rich in alanine and glycine residues with high β-sheet propensity and 11 small, more hydrophilic, charged and amorphous domains. The N terminus and all of the 11 amorphous domains contain acidic groups, while only the first and last amorphous domains and the C terminus contain basic groups, leading to a low pI value of 4.2 [5].

The sequence of the light chain is less repetitive and has a high content of glutamic and aspartic acid residues. Silk fibroin has been processed into a variety of material formats such as films, electrospun fibers, 3-D porous scaffolds, microspheres and hydrogels from an initially random-coil rich conformation in aqueous solution, mainly for tissue engineering and cell/drug delivery applications [6–12].

Silk hydrogels have been studied for potential biotechnological applications due to their exceptional mechanical properties, biocompatibility, controllable degradation rates and self-assembly into β-sheet rich networks [8,13–17]. Previously, self-assembly and subsequent hydrogelation of silk fibroin was triggered in vitro in solution conditions such as low pH, high temperatures or high ionic strength [8] or alternatively in physiologically relevant solution conditions via ultra sonication [11] or vortexing [17] for cell/drug encapsulation/delivery. In the majority of these silk hydrogel systems, the hydrated network is rich in non-covalent but essentially irreversible, intermolecular β-sheet crosslinks. In contrast, the e-gel system involves temperature reversible, dynamic self-assembly of silk [2]. This material displayed interesting viscoelastic properties, such as reversible shear stiffening at low shear amplitudes followed by irreversible stiffening at high shear amplitude. Increasing the electric field strength and/or the electrogelation duration, as well as application of elongational and/or shear forces resulted in transitioning of the e-gel into more stable hydrogels richer in β-sheet content, with remarkable changes in viscoelastic and adhesive properties.

The goal of the present paper is to provide insight into the electrogelation process with silk. Toward this goal, first we characterize the changes in rheological behavior of the silk fibroin aqueous solution associated with the electrogelation process in situ via electric field rheology to minimize previously reported dehydration and shear/elongational force effects, as well as to identify the dependence of viscoelastic characteristics on various processing conditions. Second, we compare the structure, micron-scale morphology and adhesion of e-gels with other silk hydrogel systems to develop an electrogelation model, en route to understanding the origins of unique adhesive characteristics of the e-gel system.

2. Experimental Section

2.1. Preparation of Aqueous Silk Fibroin Solutions

Silk fibroin aqueous solutions were prepared as previously described [18]. Briefly, *Bombyx mori* cocoons were boiled for 20 min in an aqueous solution of 0.02 M sodium carbonate and then rinsed thoroughly with deionized water. After overnight drying, the silk fibroin was dissolved in an aqueous solution containing 9.3 molar LiBr at 60°C. The solution was dialyzed against deionized water using Slide-a Lyzer dialysis cassettes (MWCO 3,500, Pierce) for 2 days to remove the residual salt. The final concentration of the silk fibroin was approximately 7.3 wt %.

2.2. Preparation of Silk Hydrogels

For silk hydrogelation triggered by a drop in solution pH (pH-gels), a dilute aqueous HCl solution was added into a 7.3 wt % silk solution (pH 6.4) at a 1:10 volumetric ratio to adjust the final proton concentration due to strong acid from 0.01 M (pH ~ 4) to 0.1 M (pH ~ 1.5). Sonicated gels (s-gel) were prepared according to the previously described procedure [11]; namely, 1 mL of 5 wt % silk solution kept in a glass vial was sonicated for 5 seconds using a Branson Sonifier (Danbury, CT) at 10% power setting.

2.3. In-situ Electric Field Dynamic Oscillatory Rheology

Dynamic oscillatory time, frequency and strain sweeps were performed using an ARES strain-controlled rheometer (TA Instruments, New Castle, Delaware). Twenty-five mm diameter thin platinum disks were attached to the surface of custom-machined acrylic plates, which insulated the disks from the manufacturer supplied rheometer fixtures. The platinum disks were connected to conductive wires embedded in the acrylic insulation to enable in situ application of electric field during rheological testing. In a typical experiment, the silk solution was loaded onto the bottom plate gently to prevent shearing of the sample and the top plate was lowered to a measuring gap distance of 0.5 mm. The normal force applied on the solution during lowering of the top plate was less than 0.05 N. A low viscosity mineral oil was used to prevent sample evaporation from the sides of the plate. The electric field was applied one minute after starting a dynamic oscillatory time sweep test ($\gamma = 1\%$, $\omega = 10$ rad/s). Frequency sweeps were collected over a wide frequency range ($\gamma = 1\%$, $\omega = 0.1 - 100$ rad/s). Strain sweep measurements were performed from $\gamma = 0.01 - 1000\%$ ($\omega = 10$ rad/s) to determine the linear viscoelastic regime.

2.4. Dynamic Mechanical Analysis

For DMA experiments, silk e-gels were prepared by immersion of two platinum electrodes in 0.5–1 mL of 7.3 wt % aqueous silk solution and by application of 25 VDC over a 1–4 minute period. The gel-like material that formed at the positive electrode (egel) was separated from the silk solution using tweezers. In a typical experiment, ~0.1 mL of sample was gently loaded onto the 8 mm diameter stainless steel plates of a TA Instruments RSA3 Dynamic Mechanical Analyzer (DMA) directly. The top plate was lowered to a gap of 2 mm, applying less than 0.05 N compressive force on the sample. Sample equilibration was followed by a strain-controlled dynamic time sweep test at low strain amplitude (1–5% strain at 1 Hz). Subsequently, a transient tensile test at a constant transducer speed of 5 mm/min was collected until complete de-adhesion. The sample-plate interface was observed throughout the test for possible decrease in contact area. The work of adhesion was calculated from the integral of the normal stress-strain curve [19] using TA Instruments data analysis software.

2.5. Raman Spectroscopy

E-gel samples for Raman spectroscopy were prepared using the same procedure as in DMA sample preparation. A Jasco NRS-3000 Series Laser Raman Spectrophotometer (Jasco, Tokyo, Japan) was used to obtain Raman spectra, with a 785 nm laser at a power of 180 mW. A 20x objective was employed and spectra were collected in the range of 283–1970 cm^{-1} with an exposure time of 20 sec and 10 consecutive accumulations. Spectra were then analyzed using Jasco Spectra Manager Software for the NRS-3000 Series Raman.

2.6. Polarized Optical Microscopy

For POM experiments, a drop of 7.3 wt % silk solution was applied between two platinum wires placed on a glass slide. After application of the silk solution, the wires were encapsulated between the glass slide and a cover slip and possible changes in morphology

were observed during electric field application. A Nikon Eclipse E600 Polarizing Optical Microscope (Nikon, Tokyo, Japan) connected to a CCD camera (Diagnostic Instruments, Minnesota, USA) was used to obtain images that were then analyzed using the Spot 4.09 Image Analysis Software (Diagnostic Instruments, Minnesota, USA). A 20x objective was used for all samples.

3. Results and Discussion

3.1. Electrogelation kinetics by in situ electric field rheology

Fig. 1 (a) shows the time evolution of viscoelastic properties of the silk solution in response to a stepwise increase in the applied electric field from 0 to 20 V/mm at a rate of 1 V/mm/min. The initial, low elastic (G') and loss (G”) modulus values corresponding to low applied electric fields were indicative of the initial solution state. At this stage, the viscoelastic properties of the silk solution were below the detection limit of the setup due to the small applied strain leading to high noise levels. An increase in both G' and G” was observed with increasing field strength, while the rate of increase was higher for G' than that of G”, with an apparent G'/G” cross-over at an electric field of $E_x \sim 11$ V/mm (the value of E_x decreased with increasing rate of increase in the applied field). After the apparent G'/G” cross-over, there was a gradual increase in G' values, which approached a plateau of about 300 Pa. and a simultaneous decrease in the loss tangent for electric fields greater than E_x, typical of a gelling system. The final e-gel displayed a slight frequency dependence in the measured frequency range (Fig. 1 (b)), indicating the formation of a hydrogel network via relatively long lifetime physical crosslinks between silk fibroin molecules.

Next, we investigated the kinetics of silk electrogelation at various applied electric fields to clarify the observed decrease in apparent E_x with increasing rate of increase in the electric field. Fig. 1 (c) shows dynamic oscillatory time sweeps collected from 7.3 wt % silk solutions at different applied electric fields. For electric fields ≤ 5 V/mm, there were no apparent changes in viscoelastic properties during a 100 minute test, while electrogelation was observed for fields of ≥ 7 V/mm, suggesting that a critical field of 5–7 V/mm was required to trigger electrogelation. The electrogelation kinetics increased with increasing field strength up to 15 V/mm. However, high electric field values lead to inconsistencies in the measured G' values (e.g., the drop in stiffness for the 15 V/mm sample after ca. 500 seconds) after the initial stiffening, presumably due to increased bubble formation at the electrodes. Here, it should be noted that intrinsic bubble formation in e-gels leads to an underestimation of the measured final hydrogel stiffness. On the other hand, we would not expect a significant effect of bubble formation on the measured apparent G'/G” cross-over time or E_X values.

Interestingly, the increase in stiffness due to electrogelation was accompanied by a concomitant, substantial increase in the negative normal force (e-gel pulling the rheometer plates together) (Fig. 1 (d)). Negative normal force generation was previously reported in semiflexible biopolymer networks, such as crosslinked F-actin collagen, fibrin, neurofilaments and Matrigel, due to strain stiffening behavior in response to applied shear in these systems [20]. This normal force generation was attributed to the differences in the stress response of semi-flexible biopolymer chains for different modes of applied strain (greater stress response in tension than that in compression) leading to a net negative normal force. Even though a slight strain hardening was previously observed in e-gels, the amplitude of strain applied during the current dynamic time sweeps is much lower than those corresponding to e-gel strain stiffening [2]. On the other hand, substantial negative normal force generation was also observed in electrorheological (ER) fluids [21], particle suspensions that solidify at strong electric fields on the order of kilovolts per mm. For example, Jordan et al. observed a linear dependence of the negative normal force on the

square of the electric field strength for an ER fluid, which could be attributed to the normal stress/field strength relationship in a capacitor [21], a mechanism that is possibly more relevant to silk electrogelation. However, the exact origins of negative normal force generation in e-gels need to be studied further. In addition to the negative normal force generation, electrogelation was also accompanied by a decrease in current reading, presumably due to the insulating effect of the e-gel and the increasing concentration of bubbles covering the electrode surface.

Fig. 2 shows the effects of repetitive application and subsequent removal of the electric field on the rheological behavior of e-gels. Following the initial electrogelation, removal of the applied electric field led to a decrease in the measured storage modulus. E-gel stiffness dropped from ca. 300 Pa to ca. 30 Pa in 10 minutes, suggesting partial reversibility of the electrogelation process. This apparent reversibility of hydrogel stiffness could be attributed to the dynamic nature of electric field induced physical crosslinks between silk fibroin molecules. Subsequent application of electric field led to rapid stiffening with faster kinetics than the initial electrogelation process. It should be noted that the decrease in the measured G' values immediately after the reapplication of electric field as compared to those measured immediately before the field application could be due to formation of bubbles or the build-up of negative normal force, both leading to underestimation of the measured final hydrogel stiffness, as discussed before. Increasing electrogelation kinetics during the second application of the electric field was probably due to the formation of physical crosslinks at a higher rate when compared to that during the initial electrogelation, possibly because the initial electrogel network only partially disentangled due to removal of the applied field. When the electric field was removed the second time, a decrease in the stiffness similar to that due to the first field removal was observed. Overall, the stiffness of the e-gel could dynamically be controlled and partially reversed through repetitive application and removal of electric field.

Electrogelation kinetics and the final e-gel stiffness were strongly dependent on various assembly conditions (Fig. 3) in addition to the applied field strength. For example, for an electric field of 9 V/mm, electrogelation kinetics slowed down significantly when the concentration was reduced from 7.3 wt % to 4.8 wt % with a significant drop in the final hydrogel stiffness (from >200 Pa to ca. 80 Pa) (Fig. 3 (a)). On the other hand, for a 3.6 wt % solution, there were no apparent changes in the rheological behavior within 2000 seconds, suggesting a critical minimum silk concentration for e-gel formation at a given electric field strength. Similarly, solution pH had a drastic effect on electrogelation kinetics. pH effects were only investigated at basic solution conditions, since slightly acidic ($pH \leq 5$) 4.8 wt % silk solutions gelled immediately. For a field strength of 9 V/mm, increasing the solution pH from 6.5 to 8.3 led to a four-fold decrease in the measured G' values, while no electrogelation was observed when solution pH was initially adjusted to pH 9.3. Slowing down the electrogelation kinetics with increasing pH highlights the importance of increased proton concentration at the positive electrode due to the applied field on e-gel formation.

3.2. Structural characterization by Raman and POM

Fig. 4 shows Raman spectra collected from silk solution, pH-gels ($[H^+] = 0.1$ M), e-gels and sonicated gels (s-gels) (details of sample preparation were provided in section 2). Raman data indicate clear differences between the s-gel and the other three cases (solution, e-gels and pH-gels). In the amide I region, s-gel showed a peak at around 1662 cm^{-1} that roughly corresponds to a β-sheet and random coil conformation, as prior studies have associated the peaks around 1665 cm^{-1} and 1660 cm^{-1} with the stretching of the C=O bonds along the backbone chains in β-sheets [22,23] and random coils [24], respectively. The broad shoulders in the amide I region (1600–1700 cm^{-1}) for the silk solution resembled that of the e-gel and the pH-gel, suggesting a predominantly unordered conformation [22]. In the amide

III region the peak for the s-gel at 1228 cm^{-1} can be assigned to stretching of C-N bonds consistent with a β-sheet conformation [23,25]. Once again, in the amide III region, silk solution, e-gels and pH-gels share a broader peak centered at about 1250 cm^{-1}, which along with the broad amide I peaks lends more evidence to an unordered secondary structure in these systems [22]. Besides the amide bands the s-gel Raman spectrum again differed from those collected from other three systems with a peak at 1081 cm^{-1} consistent with β-sheet conformation [22,24,25], whereas the peak around 1100 cm^{-1} for the other three systems is more indicative of the presence of random coils and turns [22]. Overall, the Raman data suggest that the s-gel is richer in β-sheet content when compared to the other three systems. This high β-sheet content could be attributed to intramolecular folding of silk molecules into β-strands followed by intermolecular assembly into β -sheet rich hydrogel networks due to sonication, in good agreement with previous results [11]. On the other hand, the overall molecular conformation of e-gels and pH-gels seem to be very similar to that of the solution state. On the other hand, the possible presence of silk I structures rich in helical interactions in both e-gels and pH-gels can not be ruled out, considering the similarity between the Raman spectral patterns of the random coil and silk I structure [24]. The lack of the previously reported, low helical spectral signature in e-gels [2] could also be due to partial disruption of helical interactions and/or partial reversal of hydrogelation due to Raman sample preparation. Overall, the Raman data suggest that e-gel and pH-gel formation is predominantly due to physical, entanglement crosslinks and possible helical interactions between silk fibroin chains that are not associated with significant β-sheet formation.

Servoli et al reported orientation of silk fibroin molecules in air dried films parallel or antiparallel to an applied AC electric field due to the net dipole moment of the silk fibroin protein, resulting from the surface charge, polar groups and mobile ions [3,26]. We studied possible similar micron- to macro-scale alignment of previously reported micron-scale spherical and elongated silk fibroin micelles [2] in DC fields and expected birefringence thereof using Polarizing Optical Microscopy (POM) [27–29]. POM images were collected from the silk solution, e-gel and pH-gel [H^+ = 0.1 M] both under normal light transmission and at maximal birefringence (cross-polarizers at 90°) (data not shown). In both cases, no structural features were observed from silk solutions, while a similar micron-scale structural heterogeneity that resembles previously observed spherical and elongated, micellar microstructures, was observed for the e-gel [2] and pH-gel. Neither e-gels nor pH-gels displayed birefringence patterns (which should appear as bright color patterns with the polarizers at 90° [27–29]) suggesting the absence of long-range alignment of silk fibroin micelles.

3.3. Adhesive characteristics

Fig. 5 shows the adhesive characteristics of silk solution, pH-gels ([H^+] = 33 mM) and e-gels on stainless steel surfaces measured by a dynamic mechanical analyzer operated in strain controlled, transient tensile testing mode. All samples displayed similar, linear stress-strain behavior at low strains (< 20%) (Fig. 5 left inset). At higher strains, sample/plate contact area progressively decreased. For the silk solution, the decrease in the contact area led to a peak in the normal force which quickly diminished at ca. 150% strain. On the other hand, both e-gels and pH-gels showed unique, non-linear adhesion characteristics when compared to other synthetic bioadhesive systems [30]. After the initial linear regime, the normal force progressively increased for both systems. For pH-gels, the non-linear regime was rather smooth, with an increasing slope despite the decreasing sample/plate interface. A similar increase in the slope of the stress strain curve was also observed for e-gels, albeit random fluctuations in stress that are attributable to trapped gas bubbles in the e-gel acting as crack nucleation sites. These defects also presumably lead to premature failure of e-gels. The increasing slope of the stress-strain curve that was observed in both pH-gels and e-gels

was presumably due to stiffening of both systems due to surface effects and elongational forces. Application of a low viscosity oil around the samples prior to adhesion testing in order to minimize possible surface effects led to a significant drop in the work of adhesion values, suggesting that surface effects play a significant role in e-gel adhesion. In all cases, very high strain-to-failure values (> 1000 %) were recorded. Even though, the measured adhesion values of e-gels reported here should be taken as a lower limit of the true intrinsic adhesive characteristics of the e-gel due to entrapped bubbles, adhesion testing results indicate that the essential adhesive properties of the e-gel could be captured by pH adjustment of the silk solution (Fig. 5 right inset shows the dependence of work of adhesion values for pH-gels on proton concentration). Interestingly, pH-gels that displayed the strongest adhesive characteristics ($[H^+]$ = 33 mM) were significantly more compliant than e-gels in dynamic shear (Fig. 1 (b)).

3.4 Electrogelation Mechanism

Fig. 6 shows a schematic of the proposed electrogelation mechanism based on combined structural and mechanical data that is summarized in Table 1. In neutral to basic aqueous solution, the acidic charged groups in the amorphous domains of the silk fibroin heavy chain prevent intramolecular β-sheet folding, while the overall negative surface charge due to these charged domains prevent intermolecular self-assembly. The dependence of electrogelation kinetics on solution pH measured by rheology and similarities between the structure and adhesive characteristics of the e-gel and pH-gels according to combined Raman, POM and DMA data suggest that the increase in proton concentration in the vicinity of the positive electrode due to the applied electric field is possibly a predominant factor in electrogelation. This local decrease in solution pH presumably leads to screening of the acidic surface charged groups enabling intermolecular self-assembly events. Dynamic shear rheology data indicated that e-gels were generally stiffer than pH-gels (Fig. 1 (b)), albeit with similar adhesive characteristics. Higher stiffness of e-gels may stem from possible molecular alignment/chain stretching of fibroin dipoles facilitating a higher concentration of intermolecular crosslinks. However, such potential electric field induced structural changes were not detectable using the current experimental techniques. Previous SEM [2] and current POM data suggest initial intermolecular assembly of silk fibroin molecules into micron-sized micelles. Moreover, it was previously observed that the overall e-gel concentration was very close to that of the silk solution [2]. The large size of micron-scale micelles as compared to that of the single fibroin molecule suggests self-assembly of amphiphilic fibroin molecules into complex micelles, in which hydrophobic interactions between repetitive domains of the fibroin could be screened by less hydrophobic, amorphous spacers that are more readily exposed to water. These micelles could be comprised of a low-density, fractal-like substructure leading to the relatively low overall concentration of the e-gel (Fig. 6). The lack of a significant increase in the β-sheet content in e-gels when compared to the solution state measured by Raman spectroscopy suggests that both the intermolecular self-assembly events leading to micelle formation and the crosslinks between these micelles leading to the observed soft-solid-like rheological behavior are mainly dominated by physical entanglements between random-coil-rich silk fibroin molecules and/or possible temperature reversible, helical interactions between the amorphous spacers in the silk fibroin chain. Rheology data indicate that these entanglements act as long lifetime crosslinks, presumably due to increased hydrophobic interactions between tangled fibroin chains. It is difficult to estimate the possible molecular weight dependence of silk electrogelation kinetics based on the current model: Increased molecular weight could increase the intermolecular entanglement crosslink density, while decreasing molecular alignment propensity with the applied field. Other factors, such as overall charge/charge distribution and solution temperature could also affect the electrogelation kinetics. For example, the removal of the negatively charged light chain could potentially decrease the

critical field for electrogelation and/or speed up electrogelation kinetics at a given field strength through a shift in the pI. These and additional factors should be the subject of further studies to refine the current model of silk electrogelation provided here.

3.5. Possible Origins of Adhesion

Several theories have been proposed to describe adhesion of two dissimilar surfaces (e.g. electronic, adsorption, wetting, diffusion (interpenetration) and fracture theories [31]). It is commonly accepted that formation of an intimate molecular contact at the interface between two adhering surfaces is a necessity for adhesion [31]. The adhesive characteristics of e-gels and pH-gels on smooth stainless steel surfaces were different than that of the s-gel. In contrast with the strong adhesion of e-gels and pH-gels, s-gels did not show any detectable adhesion. We would expect the amorphous-rich structure and the hydrophilic nature of the e-gel and the pH-gel (as compared to the hydrophobic, β-sheet rich s-gels) and their viscoelastic properties would aid in the initial wetting and formation of a good interfacial contact between the gel and the stainless steel surface. Once intimate contact is achieved, strong adhesion was presumably mainly due to adsorption, i.e., adhesion due to surface forces acting between the gels and stainless steel surface oxide layer. For both the e-gel and the pH-gel these forces could include hydrogen bonding due to the amide groups of the protein and van der Waals interactions, predominantly due to main chain and side chain polar groups, mobile ions and to a lesser extent the residual surface charge.

4. Outlook

Some adhesion theories have also been applied to bioadhesion, the attachment of synthetic and biological macromolecules and hydrocolloids on biological tissue [32]. For example, mucoadhesion, which implies adhesion to a mucosal surface, is generally accepted to involve (1) the formation of an intimate contact between the adhesive material and the mucus through wetting and swelling of the material (not necessary for a fully hydrated hydrogel), (2) interpenetration of the adhesive and mucin chains and formation of entanglements and (3) possible formation of weak chemical bonds. Hydrogel characteristics such as high hydrogen bond formation propensity, high concentration of negative charge, high polymer molecular weight to increase entanglements with the mucin chains, high polymer chain flexibility to enable penetration into the mucus network and adequate surface free energy to enable proper wetting of the mucosal surface have been shown to increase mucoadhesion [30], while additional requirements include biocompatibility, non-toxicity and other factors. The suitability of silk e-gels as mucoadhesives will be the subject of future studies as they fulfill several of the above criteria. On a further note, e-gels could find future applications in biomimetic dynamic adhesion [33] through engineering of reusability into their inherently reversible and substrate tolerant nature [2].

Conclusions

Studies aimed at addressing the main processing parameters controlling silk fibroin electrogelation were conducted. Overall, the structure and adhesive characteristics of e-gels and pH-gels were similar, highlighting the importance of pH effects in e-gel formation. On the other hand, differences in shear rheological response between the e-gel and pH-gel suggested that additional factors may be operational in silk electrogelation. Future studies on this system should investigate the effects of other factors, such as solution temperature and molecular weight on e-gel formation kinetics. In addition, the origins of e-gel adhesive properties both in air and in aqueous media are not yet clear. Overall, future biotechnological applications will require continued elucidation of the mechanisms involved to further understand and control the properties of the system.

Acknowledgments

We thank Dr. Martin Hunter and Dr. Danielle Rockwood for their help with Raman experiments. We thank Prof. Peggy Cebe for her help with the polarizing optical microscope. We thank the NIH via the Tissue Resource Center (P41 EB002520) and AFOSR for support of this research.

References

1. Cheng XG, et al. An electrochemical fabrication process for the assembly of anisotropically oriented collagen bundles. Biomaterials 2008;29(22):3278–3288. [PubMed: 18472155]
2. Leisk GG, et al. Electrogelation for Protein Adhesives. Advanced Materials. 2009
3. Servoli E, et al. Folding and assembly of fibroin driven by an AC electric field: Effects on film properties. Macromolecular Bioscience 2008;8(9):827–835. [PubMed: 18528847]
4. Inoue S, et al. Silk fibroin of Bombyx mori is secreted, assembling a high molecular mass elementary unit consisting of H-chain, L-chain, and P25, with a 6 : 6 : 1 molar ratio. Journal of Biological Chemistry 2000;275(51):40517–40528. [PubMed: 10986287]
5. Zhou CZ, et al. Fine organization of Bombyx mori fibroin heavy chain gene. Nucleic Acids Research 2000;28(12):2413–2419. [PubMed: 10871375]
6. Jin HJ, et al. Electrospinning Bombyx mori silk with poly(ethylene oxide). Biomacromolecules 2002;3(6):1233–1239. [PubMed: 12425660]
7. Jin HJ, et al. Biomaterial films of Bombyx mori silk fibroin with poly(ethylene oxide). Biomacromolecules 2004;5(3):711–717. [PubMed: 15132651]
8. Kim UJ, et al. Structure and properties of silk hydrogels. Biomacromolecules 2004;5(3):786–792. [PubMed: 15132662]
9. Nazarov R, Jin HJ, Kaplan DL. Porous 3-D scaffolds from regenerated silk fibroin. Biomacromolecules 2004;5(3):718–726. [PubMed: 15132652]
10. Vepari C, Kaplan DL. Silk as a biomaterial. Progress in Polymer Science 2007;32(8–9):991–1007. [PubMed: 19543442]
11. Wang XQ, et al. Sonication-induced gelation of silk fibroin for cell encapsulation. Biomaterials 2008;29(8):1054–1064. [PubMed: 18031805]
12. Wang XQ, et al. Silk microspheres for encapsulation and controlled release. Journal of Controlled Release 2007;117(3):360–370. [PubMed: 17218036]
13. Altman GH, et al. Silk-based biomaterials. Biomaterials 2003;24(3):401–416. [PubMed: 12423595]
14. Horan RL, et al. In vitro degradation of silk fibroin. Biomaterials 2005;26(17):3385–3393. [PubMed: 15621227]
15. Ishida M, et al. Solvent-Induced and Mechanical-Treatment-Induced Conformational Transition of Silk Fibroins Studied by High-Resolution Solid-State C-13 NMR Spectroscopy. Macromolecules 1990;23(1):88–94.
16. Jin HJ, Kaplan DL. Mechanism of silk processing in insects and spiders. Nature 2003;424(6952): 1057–1061. [PubMed: 12944968]
17. Yucel T, Cebe P, Kaplan DL. Vortex-Induced Injectable Silk Fibroin Hydrogels. Biophysical Journal 2009;97(7):2044–2050. [PubMed: 19804736]
18. Sofia S, et al. Functionalized silk-based biomaterials for bone formation. Journal of Biomedical Materials Research 2001;54(1):139–148. [PubMed: 11077413]
19. Ponchel G, et al. Bioadhesive Analysis of Controlled-Release Systems.1. Fracture and Interpenetration Analysis in Poly(acrylic acid) Containing Systems. Journal of Controlled Release 1987;5:129–141.
20. Janmey PA, et al. Negative normal stress in semiflexible biopolymer gels. Nature Materials 2007;6(1):48–51.
21. Jordan TC, Shaw MT, McLeish TCB. Viscoelastic Response of Electrorheological Fluids .2. Field Strength and Strain Dependence. Journal of Rheology 1992;36(3):441–463.

22. Rousseau ME, et al. Study of protein conformation and orientation in silkworm and spider silk fibers using Raman microspectroscopy. Biomacromolecules 2004;5(6):2247–2257. [PubMed: 15530039]

23. Sirichaisit J, et al. Analysis of structure/property relationships in silkworm (Bombyx mori) and spider dragline (Nephila edulis) silks using Raman Spectroscopy. Biomacromolecules 2003;4(2): 387–394. [PubMed: 12625736]

24. Monti P, et al. Raman spectroscopic studies of silk fibroin from Bombyx mori. Journal of Raman Spectroscopy 1998;29(4):297–304.

25. Qiu WG, et al. Wet-Spinning of Recombinant Silk-Elastin-Like Protein Polymer Fibers with High Tensile Strength and High Deformability. Biomacromolecules 2009;10(3):602–608.

26. Motta A, Fambri L, Migliaresi C. Regenerated silk fibroin films: Thermal and dynamic mechanical analysis. Macromolecular Chemistry and Physics 2002;203(10–11):1658–1665.

27. Martin R, et al. Liquid crystalline ordering of procollagen as a determinant of three-dimensional extracellular matrix architecture. Journal of Molecular Biology 2000;301(1):11–17. [PubMed: 10926488]

28. Sohn S, Strey HH, Gido SP. Phase behavior and hydration of silk fibroin. Biomacromolecules 2004;5(3):751–757. [PubMed: 15132657]

29. Xu Y, et al. Solubility and rheological behavior of silk fibroin (Bombyx mori) in N-methyl morpholine N-oxide. International Journal of Biological Macromolecules 2005;35(3–4):155–161. [PubMed: 15811470]

30. Mathiowitz, E., et al. Bioadhesive Drug Delivery Systems. In: Mathiowitz, E., editor. Encyclopedia of Controlled Drug Delivery. Wiley; New York: 1999. p. 9-45.

31. Kinloch AJ. The Science of Adhesion.1. Surface and Interfacial Aspects. Journal of Materials Science 1980;15(9):2141–2166.

32. Peppas NA, Buri PA. Surface, Inerfacial and Molecular Aspects of Polymer Bioadhesion on Soft Tissues. Journal of Controlled Release 1985;2:257–275.

33. Peattie AM. Functional demands of dynamic biological adhesion: an integrative approach. Journal of Comparative Physiology B-Biochemical Systemic and Environmental Physiology 2009;179(3): 231–239.

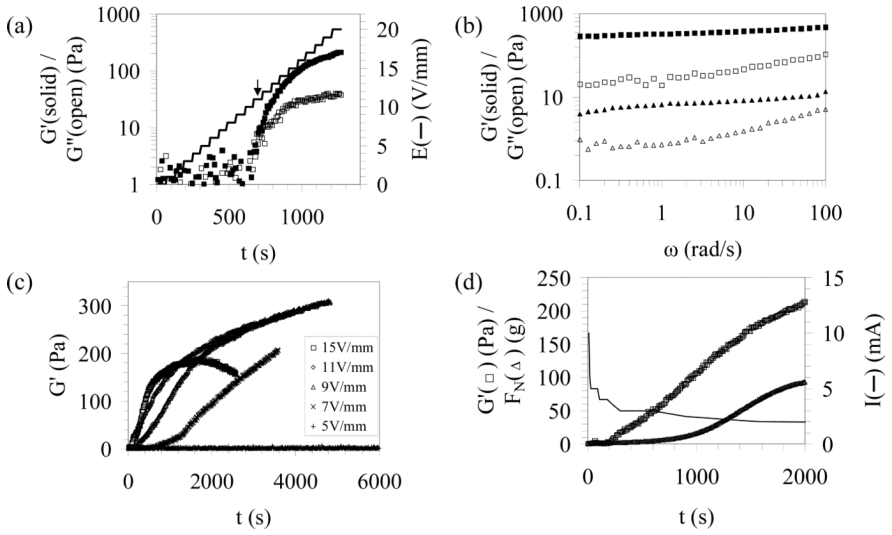

Figure 1.

In situ rheological characterization of electrogelation kinetics. (a) Change in elastic (G') and loss modulus (G") with incrementally increasing electrical field (1 V/mm/min). (b) Frequency sweeps collected from the e-gel (E = 9 V/mm) and the pH-gel ($[H^+]$ = 0.03 M). (c) Time evolution of viscoelastic properties at different electric field strengths. (d) Time evolution of elastic modulus, normal force and current at 9V/mm applied field.

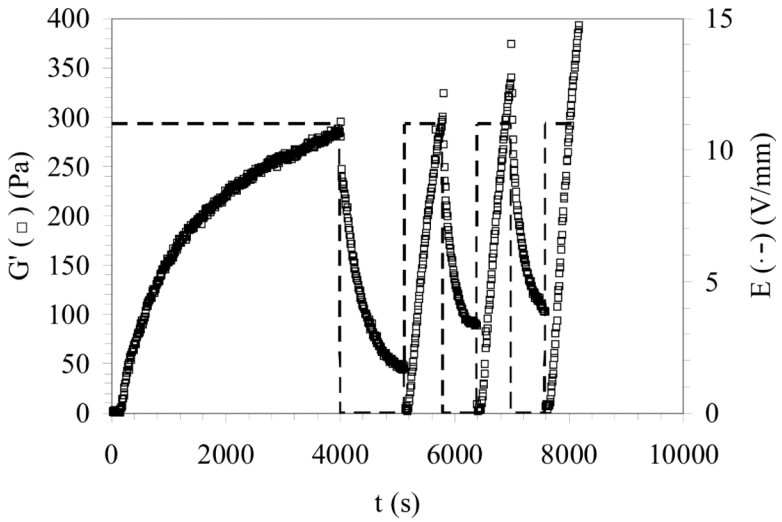

Figure 2.
Reversibility of electrogelation with application/removal of applied field.

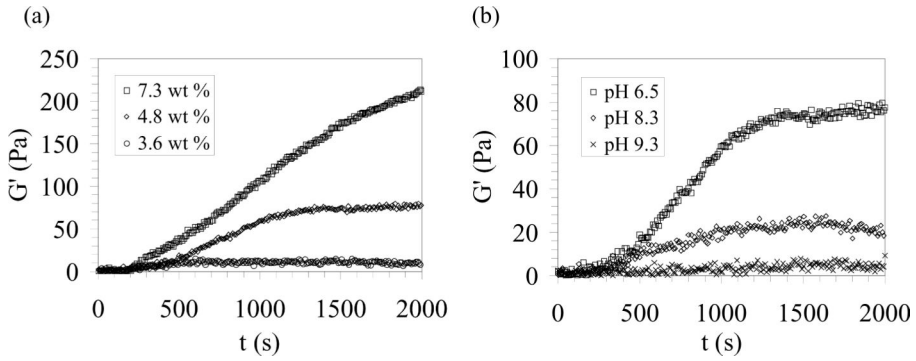

Figure 3.
Dependence of electrogelation kinetics on (a) protein concentration and (b) solution pH (for a silk concentration of 4.8 wt %) at a field strength of 9 V/mm.

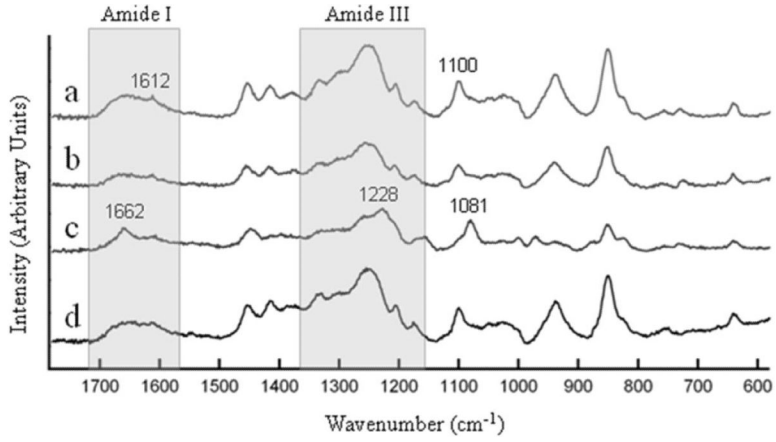

Figure 4.
Raman spectra collected from (a) e-gel, (b) pH-gel, (c) s-gel and (d) silk solution.

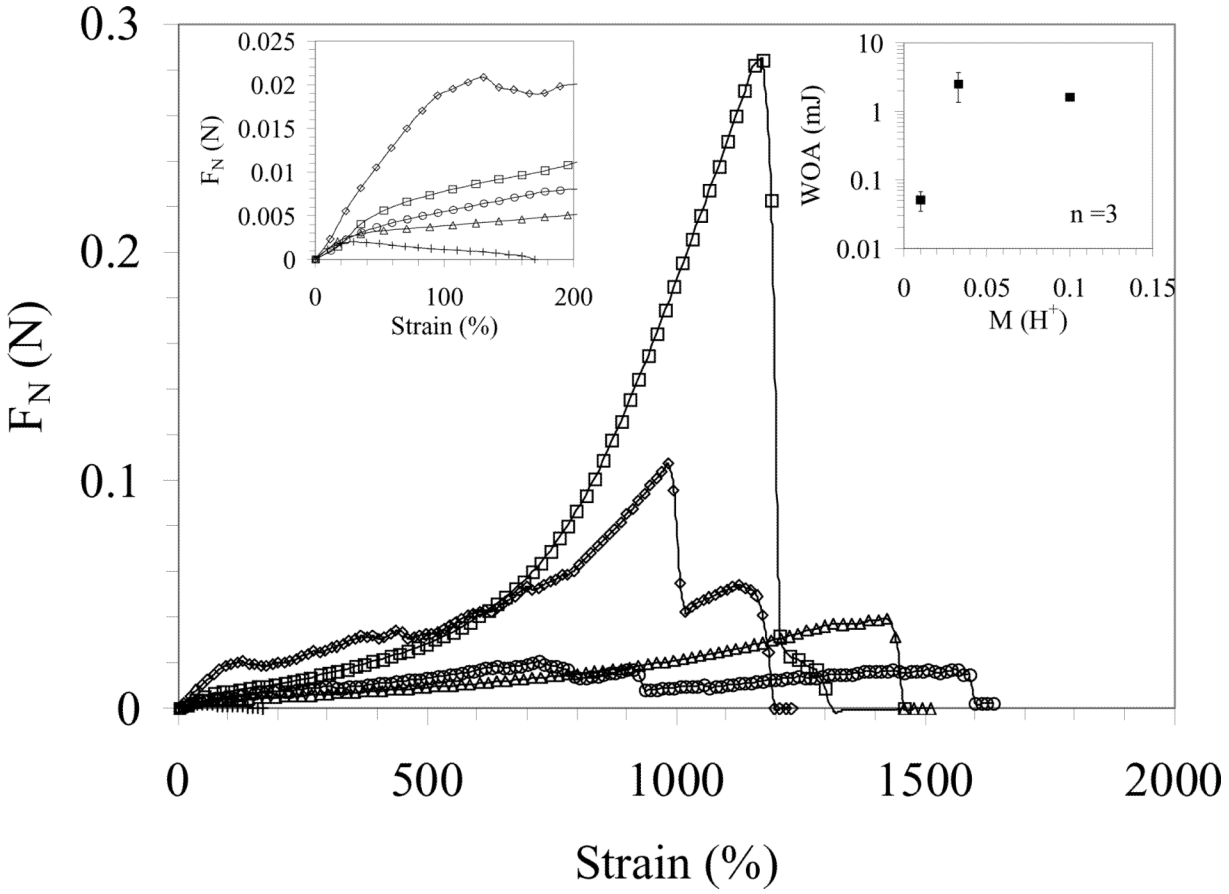

Figure 5.

Adhesive characteristics of silk hydrogels measured by DMA transient testing. (a) Engineering normal stress-strain curves for silk solution (+), e-gels (◇: no oil, ○: with oil) and pH-gels (□: no oil, Δ: with oil) on stainless steel surfaces. Left inset shows the low strain response. Right inset shows the dependence of work of adhesion values for pH-gels on proton molarity.

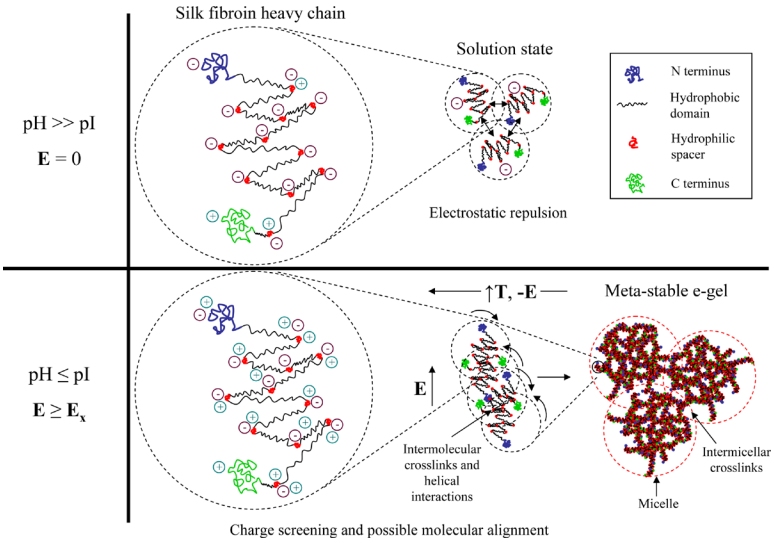

Figure 6.
Putative electrogelation mechanism

Table 1

Comparison of the structure and mechanical properties of e-gels with those of other silk hydrogel systems

	Raman peak positions (cm^{-1})			Rheology		Adhesion
	Amide I	**Amide III**	**Other**	**G' (Pa) (ω=1 rad/s)**	**Strain stiffening**	**WOA (mJ)**
e-gel	1600–1700 (broad, random)	~1250 (broad, random)	~1100 (random, turns)	~ 300	Y [2]	~ 1
pH-gel	1600–1700 (broad, random)	~1250 (broad, random)	~1100 (random, turns)	5–20	Y [2]	0.05 – 4
s-gel	1662 (β, random)	1228 (β)	1081 (β)	~ 100,000	N	~ 0